

A Comprehensive Design Guideline of Hairpin Windings for High Power Density Electric Vehicle Traction Motors

Tianjie Zou, *Member, IEEE*, David Gerada, *Senior Member, IEEE*, Antonino La Rocca, Mohsen Moslemin, Alasdair Cairns, Mengmeng Cui, Anuvav Bardalai, *Member, IEEE*, Fengyu Zhang, and Chris Gerada, *Senior Member, IEEE*

Abstract—The rapidly increasing demand on power density levels of electric vehicle (EV) drive systems is pushing the boundaries of traction motor performance. Hairpin windings are becoming a popular option for EV motors due to their reduced DC losses and improved heat dissipation capability when compared to traditional random windings. In this paper, a comprehensive design approach of hairpin winding layouts is firstly presented. The flexibility and limitation of end-winding patterns is thoroughly investigated in terms of basic pin connections, special jumpers, transposition, parallel branches, terminal positions, phase shift, winding pitches as well as slot-pole combinations. To address the challenge of much reduced practical layout options with increased slot number per pole per phase, two novel hairpin winding designs are proposed. A 160kW, 18000rpm PM traction motor featuring the new winding layout with 54-slot, 6-pole is developed using a multidomain design platform which puts special focus on the conductor size optimization. The advantages of the designed motor are clearly revealed by comparison with the more traditional 48-slot, 8-pole counterpart. Finally, a corresponding stator prototype with the proposed hairpin winding is built to validate its manufacturability.

Index Terms—Electric vehicle, interior PM motor, hairpin winding, rectangular conductor, AC losses, transposition.

NOMENCLATURE

Z_s	Stator slot number.
n_L	Total layer number of conductors in a slot.
p	Winding pole pair number.
m	Winding phase number.
q	Slot number per pole per phase.
N_{aa}	Parallel branch number per phase.
$N_{aa\ max}$	Maximum N_{aa} among available options.
N_s	Turn number in series per phase.
$N_{s\ min}$	Minimum N_s needed for winding design.
$N_{pin\ min}$	Minimum pin number in series per phase.
$N_{L\ change}$	Minimum pin number in series between layer change in hairpin winding layout.
$N_{q\ change}$	Minimum pin number in series between phasor change in hairpin winding layout.
$N_{revo\ change}$	Minimum pin number in series between revolution change in hairpin winding layout.
τ_p	Pole pitch of the winding.
S_i	The i_{th} slot in hairpin winding layout.
L_j	The j_{th} conductor layer in winding layout.
x_c	Serial number of current pin.
y_c	Serial number of next pin to be connected.

I. INTRODUCTION

WITH the global drive of pursuing “Net Zero” to deal with climate change and emissions reduction, the electrification trend is irreversible within the transportation industry [1-2]. Many countries and automotive companies have set timelines to terminate the sales of conventional vehicles within the next decade [3]. These ambitious commitments translate to significantly improved performance requirements on power trains in pure/hybrid electric vehicles (xEVs) [4-6], at the very heart of which there is the electrical machine. The fundamental competitiveness of electrical machine developments is mainly embodied in the ability to achieve high power density (kW/kg or kW/L), high efficiency, together with the all-important cost-performance (\$/kW).

As illustrated in Fig. 1, both the USA’s Department of Energy (DoE) and the UK’s Advanced Propulsion Centre (APC) have set motor-level improvements to be achieved by 2025 which are a step change with respect to any motor currently used within commercial xEVs [4-6]. In a way this is pushing the boundaries of next-generation traction motor developments in terms of increasing both torque density and rotational speed [7]. Torque density is directly related to the motor’s magnetic and electric loadings. High magnetic loading provided by strong permanent magnets (PM) and ferromagnetic materials have made the PM motor the topology of choice for EV traction. Meanwhile, high current loading generally corresponds to high power loss and brings challenges in thermal management. On the other hand, increase of rotation speed also brings additional losses and is restricted by the rotor’s mechanical strength, as well as switching capability of power electronic inverters.

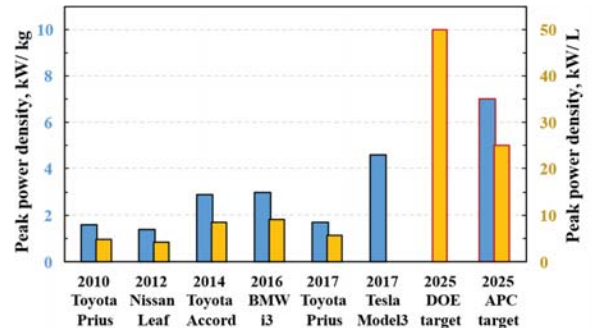


Fig. 1. Published peak power density data of existing EV/HEV traction motors and future roadmaps (continuous values given in APC roadmap) [1], [4-6].

Corresponding Author: Tianjie Zou, T. Zou, D. Gerada, A. La Rocca, M. Moslemin, A. Cairns, M. Cui, A. Bardalai, F. Zhang, and C. Gerada are with the Power Electronics, Machines and Control (PEMC) group, University of Nottingham, NG7 2GT. Email: tianjie.zou@nottingham.ac.uk; david.gerada@nottingham.ac.uk; a.larocca@nottingham.ac.uk; mohsen.moslemin@nottingham.ac.uk; alasdair.cairns1@nottingham.ac.uk; mengmeng.cui@nottingham.ac.uk; anuvav.bardalai@nottingham.ac.uk; fengyu.zhang@nottingham.ac.uk; chris.gerada@nottingham.ac.uk.

Windings housed within stators are the “central pivot” of electromechanical energy conversion, operating at inherently higher temperatures due to DC and AC copper losses, which to a large extent determine the motor’s power density level. Early generation xEV traction motors such as Toyota Prius 2010 and Nissan Leaf- 2012 adopted stranded round wires to form stator windings [8]. Although these small sized wires are with negligible skin and proximity effects at the “strand level”, at high speed operation there might be significantly increased AC losses at “bundle level” due to circulating currents between parallel strands [9].

The ever increasing requirements on power density and efficiency of traction motors have prompted a revolution of winding technologies. Hairpin windings with rectangular conductor bars are gradually replacing random windings in xEV industry [10]. An inherent advantage of hairpin winding over stranded round wires is the high slot fill factor and hence much reduced DC resistance and loss. More importantly, with significantly improved uniformity/accuracy of conductor placement in and out of slots, enhanced cooling techniques could be applied to effectively increase current density/loading which further boosts power density. This type of winding was first proposed by Dr. Cai [11,12], and consists of rectangular shaped conductor bars aligned as single array along the depth of the stator slots. Since then, hairpin winding has been subsequently applied in popular HEVs including the Chevrolet Bolt/volt [13] and Toyota Prius [14].

Research activities on hairpin windings in recent years have mainly focused on electromagnetic design [15-17], AC losses [18-20], thermal management [21-23], insulation properties [24, 25] as well as manufacturing process [26-28]. Quantitative performance comparisons were made in [10, 15] which highlighted the advantages of hairpin windings over random windings. Novel AC resistance/ AC loss modelling of rectangular conductors were proposed based on analytical [18], hybrid [19] and FEA [20] methods in order to balance computation time and accuracy. Advanced cooling arrangements were investigated including direct inner cooling [21] and end winding spray [22, 23]. Partial discharge and insulation reliability were also discussed in [24, 25] to evaluate dielectric properties of rectangular conductor bars. Moreover, automated bending [26], laser welding [27], grooving [28] as well as error detection [29] have also been looked into with an aim to improve the manufacturing procedures .

It should be noted that hairpin winding layout design is the foundation of all the research topics above. Proper transposition is essential to eliminate potential circulating current between parallel branches [30, 31]. On this basis, the end winding connection should be as uniform as possible to reduce the number of pin shapes needed. Many automotive companies have filed corresponding patents [32-35] with specific end winding patterns. In [30], general layout design approaches of hairpin windings were presented, which focused on basic rules of pin connections within one branch. Thereafter, asymmetric hairpin windings were further proposed which feature multiple pin shapes [36], variable turn number [37] and conductor splitting [38].

In this paper, a further extended and comprehensive design guideline of hairpin winding layouts is developed targeting EV traction motor applications, with flexibility and limitations

highlighted when compared to conventional lap windings. The diversity of end winding patterns is thoroughly investigated. Importantly, two novel hairpin winding designs with increased slot per pole per phase number are proposed. The advantages of the new hairpin winding designs in both electromagnetic and thermal performance are verified taking a 160kW, 18000 rpm interior PM (IPM) traction motor design as an example.

This paper is organized as follows: the basic rules and illustration of end winding connections are introduced in Section II. Then, the diversity of winding layouts in terms of basic pin connections, special jumpers, transposition, parallel branches, terminal positions, phase shift as well as winding pitches, are comprehensively summarized in Section III. Section IV is devoted to the proposal of two novel flexible hairpin winding designs which address the limitations of existing layout options. The development of a corresponding 54-slot, 6-pole IPM motor with the proposed windings is discussed in Section V, with the manufacturing process of the prototype subsequently described in Section VI for validation.

II. BASIC DESIGN RULES OF HAIRPIN WINDING

The basic concept of hairpin windings could be explained through Fig. 2, which shows a photo of conductor sample that corresponds to the stator prototype presented in this paper. The term “hairpin” is used (but not limited) to describe the conductor bent into a “U-shape”, which consists of two legs extending parallelly and can be inserted axially into stator slots from one end of the motor. With precise CNC manipulation, the legs from a series of hairpin conductors can locate at specific circumferential (different slots) and radial (different layer in one slot) positions based on carefully designed winding layouts. After the insertion the hairpin conductor legs extrude out from the opposite end of the stator and are further twisted along either the same or reverse direction. With appropriate spanning pitch, each conductor leg is then aligned and adjacent to another. Finally, all neighboring conductor legs are welded in pairs to complete the connection of phase branches.

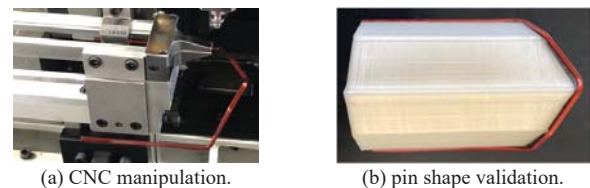


Fig. 2. Photos of hairpin shaped conductor sample used for prototyping.

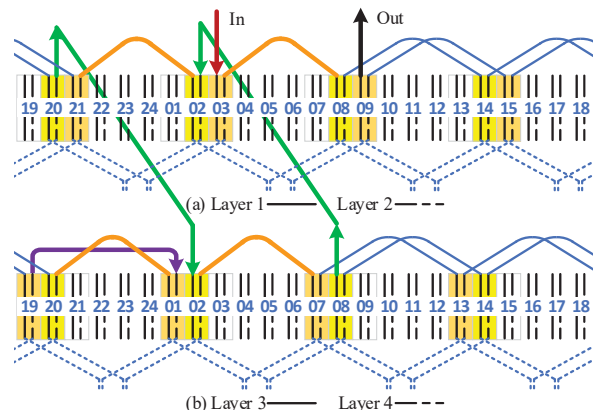


Fig. 3. Layout view of a 24-slot, 4-pole, 4-layer hairpin winding design from top side.

Layout plots are generally needed to intuitively explain the connection logic of hairpin windings. Fig. 3 shows the typical illustration method of a 3-phase, 4-layer hairpin winding layout design viewed from top side, for a 24-slot, 4-pole stator. According to Eqn. (1), the number of slots per pole per phase $q=2$. The black lines represent conductor legs (pins) located inside slots. Besides, all the other solid lines with different color denote preformed connections, while dashed lines show connections through welding from the other axial end. In this specific design, the parallel branch number per phase $N_{aa}=1$, and the turns in series per phase $N_s=16$ according to Eqn. (2). It can be seen that starting from first layer of slot number 3 (described as S_{03-L_1}), the connections from insertion and welding sides follow a wave winding pattern along the periphery of the stator, and cover the pins from layer L_1 and L_2 in an alternating way with full coil pitch. Then, a special short pitch connection from S_{21-L_2} to S_{02-L_1} (defined as 'jumper' in this paper) marked as orange is needed to change phasor. After a second round of circumferential connections, another jumper marked as green is needed to change from layers L_1, L_2 to L_3, L_4 . The same revolution is repeated with a phase shift of one slot till the pin located in S_{19-L_4} . Thereafter, a jumper with purple color achieves a single layer connection between S_{19-L_4} and S_{01-L_4} , and then followed by another round of revolution which finally goes back to S_{09-L_1} as end of branch.

$$q = Z_s / (2mp) \quad (1)$$

$$N_s = (Z_s n_L / 2) / m N_{aa} = n_L p q / N_{aa} \quad (2)$$

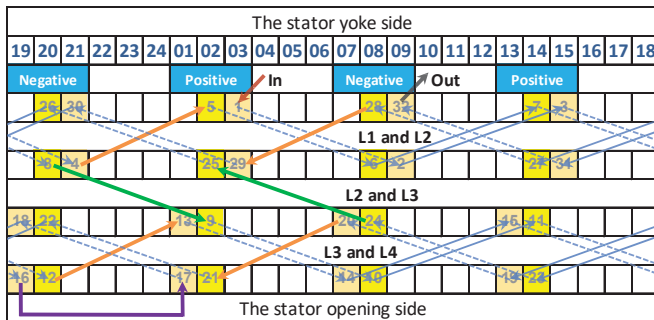


Fig. 4. Winding layout view of a 24-slot, 4-pole, 4-layer design from insertion side.

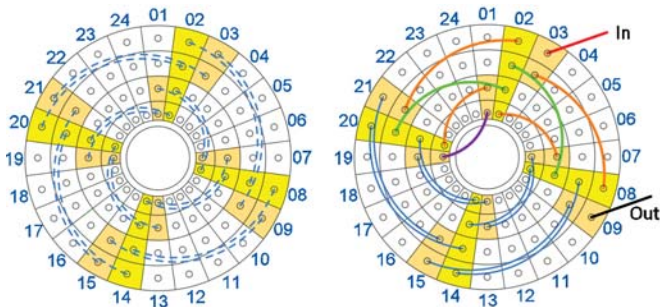


Fig. 5. Circular winding layout view of a 24-slot, 4-pole, 4-layer design from both welding and insertion sides.

Fig. 4 and Fig. 5 show exactly the same design of Fig. 3, using different illustration methods to describe the winding layout more. Fig. 4 gives a view from the insertion side, with corresponding serial number of pins to be connected. Fig. 5 presents the winding layout more from the electric machine perspective, with relative positions of pins shown clearly in

both radial and circumferential direction. These two illustrative methods will be used in a jointly way to explain more complex winding layouts within this paper.

Taking the typical hairpin winding layout designs shown above as well as based on existing research work [30], the basic configuration principles/rules for one phase of hairpin winding can be listed as follows [30-31]:

Rule#1 : Classical AC winding theory should be agreed with in terms of coil pitch selection, phase number determination, and phase belt division.

Rule#2 : Wave winding pattern should be followed, with connections travelling circumferentially to cover all poles, phasors, and layers.

Rule#3 : Connections on one axial end should be purely uniform, while on the other axial side these should be as uniform as possible to reduce the manufacturing cost.

It should be noted that there are two options for Rule#3 based on which axial end to be more efficient in manufacturing. Option one is to make the welding side purely uniform, so that the twisting and welding processes can be simplified and highly automated. Taking the design shown in Figs. 2-4 as an example, the welding connections denoted by dashed lines are all identical with the same spanning direction and coil pitch. It can be also seen that in this case there are relatively more preformed pin shapes needed on the insertion side, with several jumpers. Each pin shape may correspond to one specific CNC production line to speed up manufacturing. On the other hand, option two is the other way around, with the insertion side being purely uniform and the welding side being more complex. All the following winding layouts described in this paper corresponds to option one by default, with option two easily deducible due to the mirror symmetry.

When the parallel branch number per phase $N_{aa} > 1$, there is another important rule which is called transposition [11, 12]. More specifically:

Rule#4 : Each parallel branch should include pins from all layers and cover all phasors of corresponding phase.

Rule#5 : Between different branches the number of pins in each layer as well as pins with each phasor should be identical.

Essentially, transposition needs to be achieved by configuring suitable jumpers, as the conductors located in different layers or phasors (slots) are with different impedance. This difference is caused by both AC effect on conductor resistance as well as by slot leakage inductance. Without transposition there would be considerable circulating current between branches which further leads to increased AC winding losses. Based on rules #4 and #5, the minimum number of pins N_{pin_min} or turns N_{s_min} to be connected in series is then determined from Eqn. (3), and the corresponding maximum parallel branch number per phase N_{aa_max} is calculated from Eqn. (4) [30]. Basically, at least one full revolution, defined as a group of connections travelling across all poles and then all conductor layers from top to bottom (or bottom to top), is needed in a fundamental branch. If the number of included pins within one revolution is a multiple of q , then a minimum branch could be configured within this revolution. Otherwise, more

revolutions would be needed to satisfy rules #4 and #5. In summary, most connections in a hairpin winding layout are identical to reduce manufacturing cost, while a small number of jumpers are definitely needed when there are parallel branches.

$$N_{pin_min} = LCM(n_L \times p, q), \quad N_{s_min} = N_{pin_min} / 2 \quad (3)$$

$$N_{aa_max} = \frac{Z_s n_L / m}{N_{pin_min}} = \frac{pq n_L}{N_{s_min}} \quad (4)$$

Based on the foregoing discussion, all the basic pin connections for full pitch hairpin windings with $q=2$ can be summarized as in Fig. 6 and Table I, in which all jumper connections in terms of phasor change, layer change, phasor + layer change, as well as single layer connections, are clearly clarified.

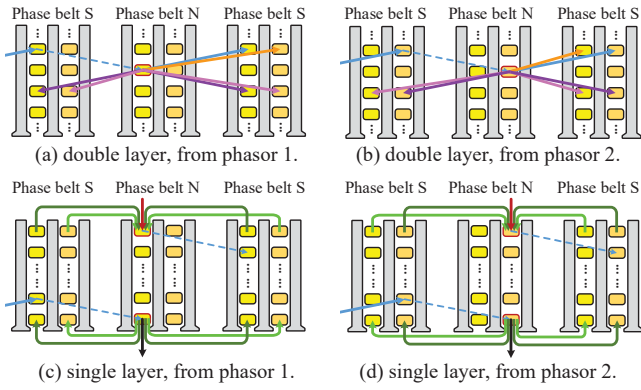


Fig. 6. Basic pin connections for multi-layer hairpin winding with $q=2$.

Table I. Classification of basic pin connections for hairpin winding with $q=2$.

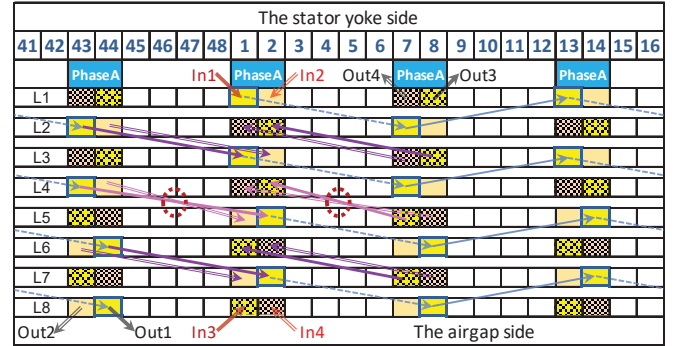
Line type	Relative position of y_c-x_c	Serial number of the prior pin	Connection type
\dashrightarrow	$=Z + \tau_p$	$2kZ < x_c \leq (2k+1)Z$	uniform winding, full pitch.
\rightarrow	$=-Z + \tau_p$	$(2k+1)Z < x_c \leq (2k+2)Z$, $k=0, 1, 2, \dots, (n_L-1)/2$, $ii=1, 2, \dots$ i.e., bias from full pitch.	double layer insertion, full pitch.
\rightarrow	$=-Z + \tau_p \pm ii$		double layer insertion, only phasor change.
\rightarrow	$=Z \pm \tau_p$		double layer insertion, only layer change.
\rightarrow	$=Z \pm \tau_p \pm ii$		double layer insertion, layer + phasor change.
\rightarrow	$=\pm \tau_p$	$0 < x_c \leq Z$, or $(n_L-1)Z < x_c \leq n_L Z$	single layer insertion, full pitch.
\rightarrow	$=\pm \tau_p \pm ii$		single layer insertion, phasor change.

From Fig. 6, it can be noted that the connection flexibility embodies mainly on the insertion side. Most connections on this side follow the pattern of the solid blue lines, with only a few jumpers as represented by solid lines in other colors. Fig. 6(a) and (b) give the connection options for intermediate layers, while Fig. 6(c) and (d) highlight the possible jumpers from first or last layer. The red and black solid lines denote pins that form terminals and neutral points, respectively. For chorded cases or increased number of q , these connection options can be extended in a similar way.

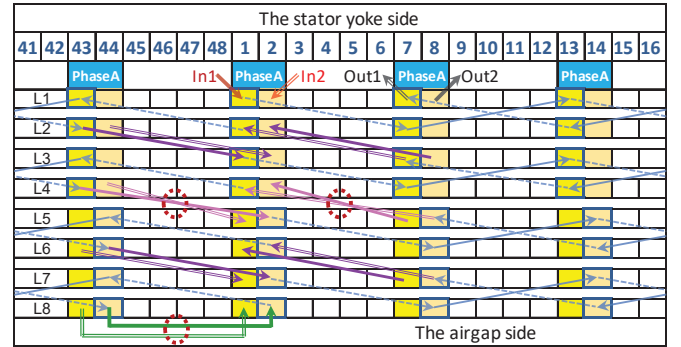
When the first pin of a branch inserted from phase terminal is identified as pin No. 1, the other pins could be numbered based on the slot number and layer number according to the wave winding pattern. By way of example, the second pin to be

connected with first pin shown in Figs. 2-4 can be marked as No. $(1+24+6)=$ No. 31. With this rule, all the pin connections could be further distinguished as shown in Table I, with x_c and y_c denoting the serial number of the current and subsequent pins to be connected.

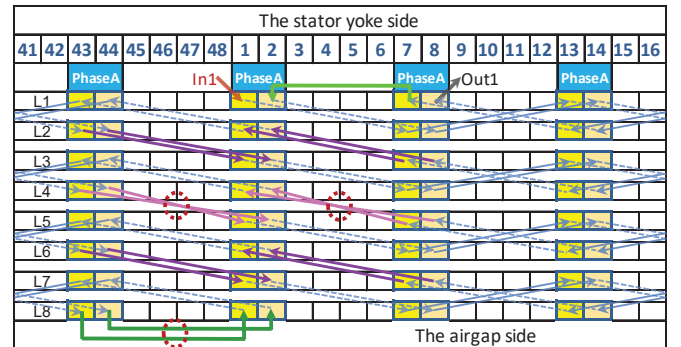
Moreover, it is also necessary to identify where the jumpers would be needed. For the case of maximizing parallel branches, the number of pins to be connected before the next jumper connection can be calculated as Eqn. (3)-(5) based on the design rules #4 and #5, where N_{L_change} , N_{q_change} and N_{revo_change} are the minimum number of pins to be connected prior to layer change, phasor change and revolution change, respectively. When $N_{L_change}=N_{q_change}$, the next pin connection on the insertion side would be both a layer as well as a phasor change. When $N_{revo_change}=N_{q_change}$, a single-layer connection with phasor change would follow. By combining Table I and Eqn. (3)-(5), a complete branch design of basic hairpin winding layout can be confirmed.



(a) phase winding layout with 4 parallel branches.



(b) phase winding layout with 2 parallel branches.



(c) phase winding layout with 2 parallel branches.

Fig. 7. Basic full pitch hairpin winding layout designs with different parallel branch number. $Z_s=48$, $p=4$, $n_L=8$, $q=2$.

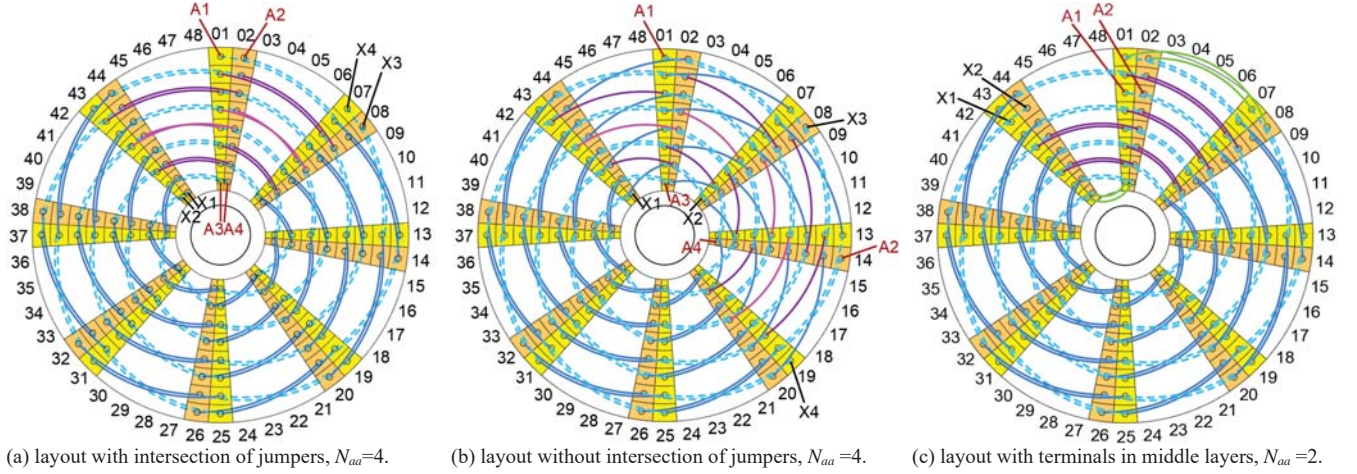


Fig. 8. Configuration of branch terminal positions for full pitch hairpin winding layouts with 48-slot, 8-pole, 8-layer.

$$N_{L_change} = \frac{N_{pin_min}}{n_L / 2} \times (1, 2, \dots, \frac{n_L}{2} - 1) \quad (5)$$

$$N_{q_change} = \frac{N_{pin_min}}{q} \times (1, 2, \dots, q - 1) \quad (6)$$

$$N_{revo_change} = pn_L \times (1, 2, \dots, \frac{N_{pin_min}}{pn_L} - 1) \quad (7)$$

With configuration rules of different jumpers identified, more complex hairpin winding layouts corresponding to practical traction motor solutions could be developed. Fig. 7 shows a corresponding 8-layer winding design with 48-slot, 8-pole, and $N_{aa_max}=4$. In Fig. 7(a), only one branch connection is shown, with covered pin locations bolded, while all jumpers from other branches are also highlighted. Figs. 7(b)-(c) give the layout design with reduced parallel number by simply connecting the minimum branches in series via the single layer jumper connection. It should be noted that there are intersections between jumpers from different phases, which need to be carefully considered as it may lead to increased difficulty in terms of practical manufacturing implementation. This issue will be further discussed in the next section.

III. DIVERSITY OF WINDING LAYOUT DESIGN

In the previous Section II, the hairpin winding layout design for one elementary branch was introduced, which is focused on basic combination of feasible pin connections, with adoption of jumpers highlighted for the purpose of transposition. With 48-slot, 8-pole designs as examples, this section will further investigate the diversity of phase winding options whilst sifting out promising layout candidates for improved performance and reduced cost.

A. Terminal positions of different branches

Generally, the terminal position of a single branch of phase winding is located at the first or last layer, which could be configured in any of the corresponding phase belts. With the first branch terminal assigned, there will be options in terminal arrangement of other branch terminals. Fig. 8(a) shows the same design of that in Fig. 7(a) with circular layout view and all other connections for one phase added. It can be seen that all the four terminals could be from one phase belt. However, there will be intersection of jumpers accordingly in such case. Based

on the following discussion in this part, it will be concluded that the terminals position of different branches could be flexibly arranged at different circumferential or radial positions in the winding layout.

As discussed in the previous section, branch 1 from A1 to X1 covers one full revolution from top to bottom layer and includes the minimum number of pins ($N_{pin_min}=32$ in this case) needed for transposition. According to Eqn. (3)-(4), there should be a jumper (solid lines in light purple in Fig. 8) following the 16th pin to achieve both phasor and layer change. As the terminal A1 locates at the left side of the phase belt, this jumper needs to follow a long pitch of 7 slots to connect the pin with the other phasor. Similarly, branch 2 from A2 to X2 follows the same connection pattern while the corresponding jumper is with short pitch of 5 slots. Since A1 and A2 locate in neighboring slots, the long and short pitch jumper inevitably overlap with each other. The same situation applies for the other branches A3-X3 and A4-X4. From a 3D modelling point of view, this could be achieved by axially separating the two jumpers to avoid interference, as shown in Fig. 9(a). It can be predicted that with increased layer or phasor number per phase, this kind of overlapping would increase challenges in manufacturing. One way to eliminate this intersection is shown in Fig. 8(b), in which A2 is arranged in another phase belt, shifted by one or more pole pairs compared with A1. Despite the benefit of separating the jumpers, the bus bars to parallelly connect A1-A4 as overall phase terminal will be much longer and increase both the cost as well as winding losses.

Apart from the flexible options on circumferential positions, branch terminals could also be assigned in different radial layers. When an even multiple of revolutions is configured for one branch, the terminal positions could be configured in intermediate layers. Fig. 8(c) gives an example with 64 pins connected and 2 revolutions in series to form one phase. In this case, the branch terminals and neutral points could be in layer L₃-L₂, L₅-L₄, or L₇-L₆, respectively. This kind of configuration is beneficial when the space near the stator yoke or airgap is too limited to put the bus bars. Moreover, when there are multiple revolutions in a branch, it is beneficial to assign overlapping jumpers with single layer connections, as the light green solid lines denote in Fig. 8(c), with a corresponding hairpin winding product shown in Fig. 9(b).

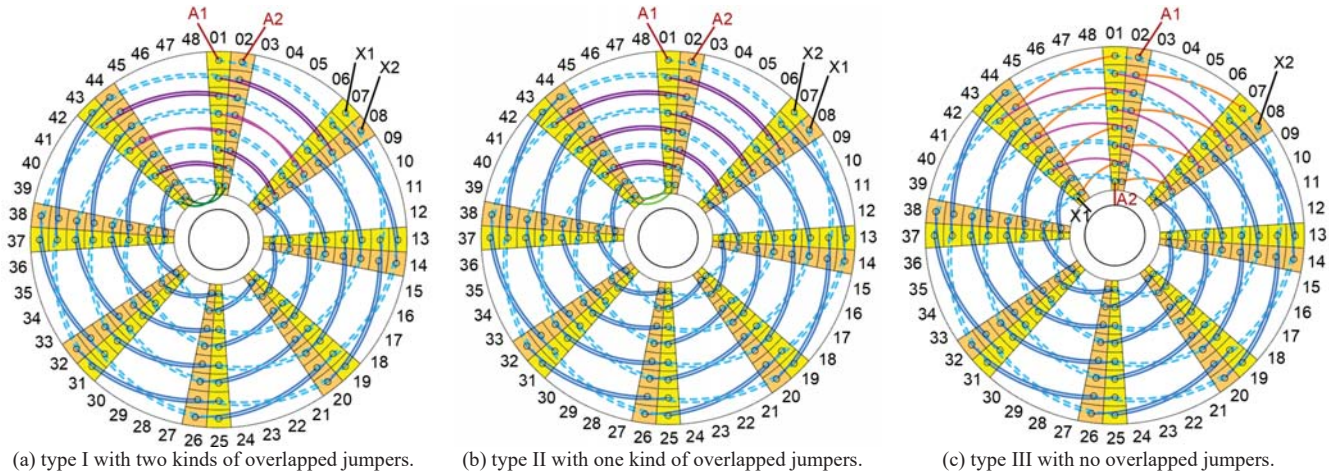


Fig. 10. Three types of jumper configuration for full pitch hairpin winding layouts with 48-slot, 8-pole, 8-layer, $N_{aa}=2$.

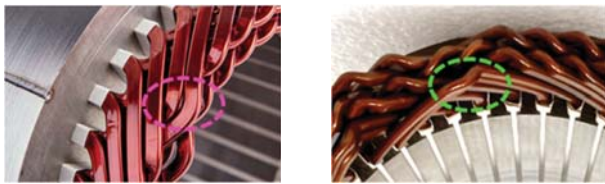


Fig. 9. Existing hairpin winding designs with overlapped jumpers.

B. Arrangement of jumpers and transposition

Based on specific slot-pole-layer combination, there could be many feasible hairpin winding solutions with different number and order of jumpers, which provides diversity in layout design. The three types of jumper arrangements for layer change, phasor change and revolution change based on Eqn. (5)-(7) correspond to the most fundamental case, with minimum number of each jumper needed for transposition. The sifting of more promising candidates out of these options is mainly driven by manufacturing cost and reliability.

Fig. 10 gives three typical 48-slot, 8-pole, 8-layer winding designs with the same electromagnetic configuration but different jumper arrangements. Fig. 10(a) corresponds to the same design concept as that in Fig. 8(a), with parallel branch number reduced by half. This is simply achieved by identifying the minimum elementary branches according to Eqn. (3)-(4), and then connect these branches in series or parallel with additional jumpers according to specific N_s needed.

However, as discussed above, either overlapped jumper connections or increased busbar lengths might be needed for this type I connection. Moreover, there are three times of phasor change from A1 to X1 and A2 to X2, which is in fact not necessary as $q=2$. Fig. 10(b) shows the improved layout type II, with only one jumper of phasor change arranged at the bottom layer for each branch. Meanwhile, Fig. 10(c) gives another option which does not need any overlapped jumpers. Different from the design concept in type II in terms of minimizing the number of jumpers, phasor changes (denoted by solid lines in orange) are assigned between every two neighboring layers before moving to the next layers. Hence, this layout type III follows the design logic of first covering phase belts (poles), then phasors and finally layers.

With a low layer number, layout type III could be more preferred than case II. While with increased layer number

which is the trend for EV traction motors, type III will lead to increased number of preformed conductor shapes and more complex busbars compared with type II. It should be noted that the jumpers for layer and revolution change in Fig. 10 (solid lines in light and dark purple) follow the same direction as that of the overall layout connection (clockwise from first to last layer and anti-clockwise backwards). Meanwhile, these jumpers can be arranged in the other directions, as illustrated in Fig. 6, with their function unchanged. The direction of these jumpers would only make some difference in manufacturing.

To distinguish the two typical winding layout type II and III, corresponding 3D models of both insertion and welding side have been established for more intuitive illustration and shown in Fig. 11. These two cases are identical for the majority of the insertion side as well as the whole welding side.

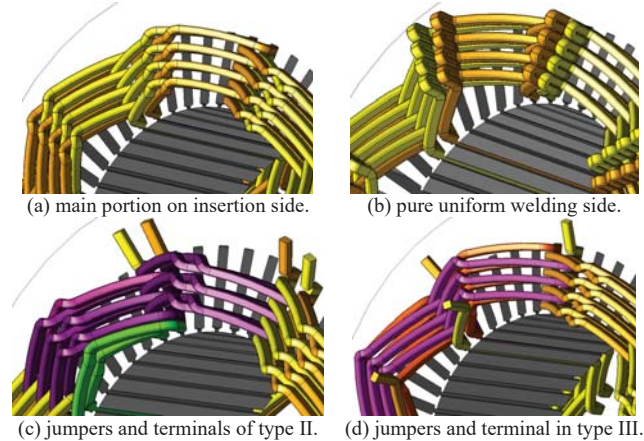


Fig. 11. 3D phase winding modelling of layout type II and III, with 48-slot, 8-pole, 8-layer, $N_{aa}=2$.

C. Phase shift and coil pitch variation

All the winding layout cases discussed above are with full pitch to highlight basic design rules. Nevertheless, short pitch windings are widely adopted for traction motors with the benefit of reduced armature reaction magnetomotive force (MMF) harmonics. Compared with randomly wound lap winding, it is more flexible to obtain short pitch designs for hairpin winding by taking advantage of its multi-layer property. Apart from setting the coil pitch unequal to pole pitch, phase shift is another way of achieving equivalent short pitch.

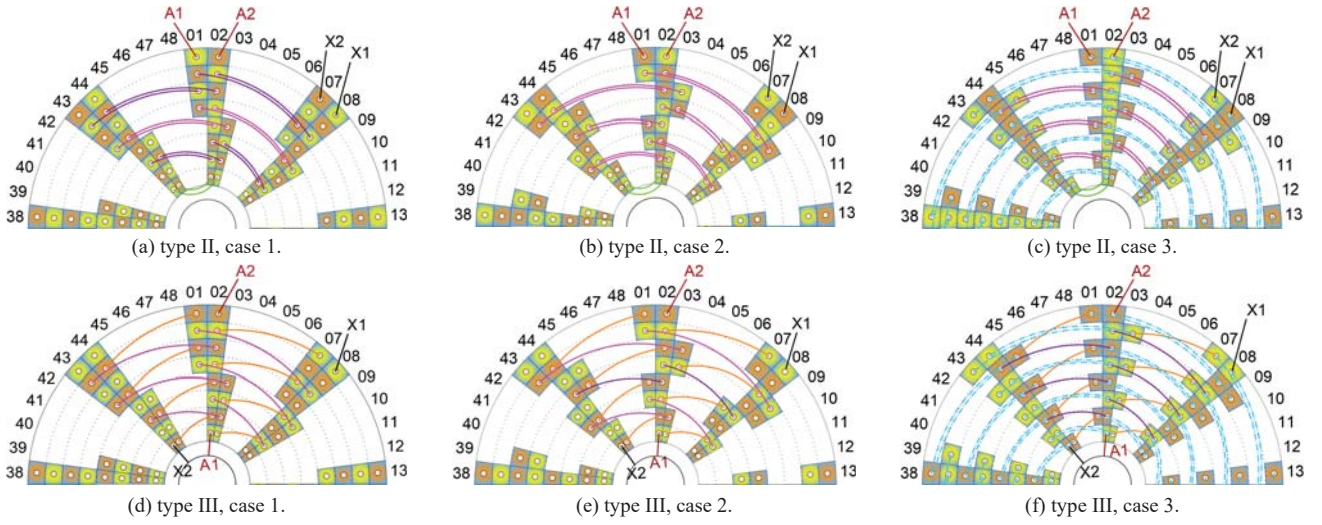
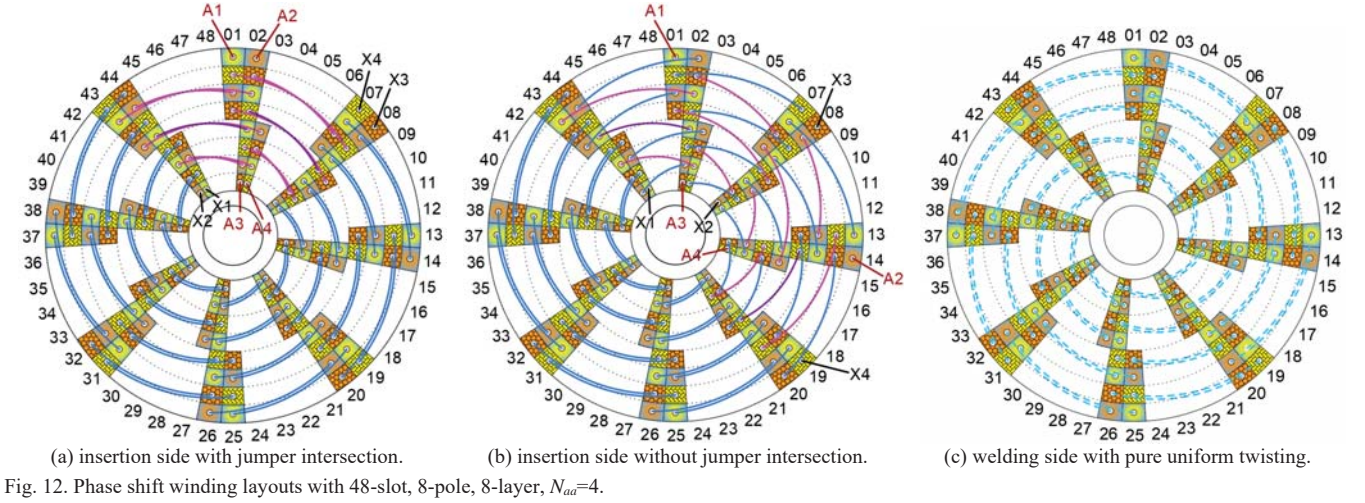


Fig. 12 shows two phase shift designs which are variants of the layouts shown in Fig. 8(a) and (b) and belong to layout type I in Fig. 10. The corresponding slots and layers are shaded by 4 patterns to indicate the pins from different branches. All welding and conventional insertion connections are with full pitch and omitted in the figure, with only terminals and jumpers highlighted. It can be clearly seen that there is a phase shift from L_4 to L_5 , which makes the whole phase winding equivalent to a one-slot short pitch design. With $N_{aa}=4$, there is only one revolution from top to bottom layer in one branch. Hence, the jumper design needs to be divided into three parts, which correspond to transposition within the first half (L_1 - L_4), second half (L_5 - L_8) of layers, and pins for phase shift, respectively.

Fig. 13 further shows the one-slot short pitched designs with $N_{aa}=2$, which are variants of the layouts shown in Fig. 10(b) and (c). Fig. 13(a) and (d) illustrate the cases with one round of phase shift from first to last layer, which correspond to the layout type II and III discussed above, respectively. Through increasing the jumper pitch between L_4 and L_5 (denoted by light purple lines) by one slot, the full pitch design in Fig. 10(b) could be transformed to that in Fig. 13(a). Similarly, the jumper pitch of 8 slots between L_4 and L_5 in Fig. 13(d) leads to the phase change for layout type III and achieves an equivalent short pitched design.

Table II. Summary of layout characteristics

Layouts	Type II, case 1			Type III, case 1		
Pin type	shapes	number	pitch	shapes	number	pitch
Regular	4	4*48	6	4	4*48	6
Layer change	2	2*12	6	0	-	-
Phasor change	0	-	-	4	4*6	5
Layer + Phasor	1	1*12	7	3	3*6	7
Single layer	2	2*3	5 and 7	0	-	-
Layouts	Type II, case 2			Type III, case 2		
Pin type	shapes	number	pitch	shapes	number	pitch
Regular	4	4*48	6	4	4*48	6
Layer change	0	-	-	1	1*6	6
Phasor change	0	-	-	4	4*6	5
Layer + Phasor	3	3*12	5 and 7	2	2*6	7
Single layer	2	2*3	5 and 7	0	-	-
Layouts	Type II, case 3			Type III, case 3		
Pin type	shapes	number	pitch	shapes	number	pitch
Regular	4	4*48	5	4	4*48	5
Layer change	0	-	-	3	3*6	6
Phasor change	0	-	-	4	4*6	5
Layer + Phasor	3	3*12	5	0	-	-
Single layer	2	2*3	5 and 7	0	-	-

TABLE III
TURN NUMBER IN SERIES PER PHASE N_s IN TYPICAL WINDING CONFIGURATIONS FOR HIGH POWER TRACTION MOTORS

Slot-pole $N_{aa} \backslash n_L$	$Z=36, P=3, q=2$				$Z=48, P=4, q=2$				$Z=54, P=3, q=3$				$Z=60, P=5, q=2$			
	4	6	8	10	4	6	8	10	4	6	8	10	4	6	8	10
1	32	48	64	80	32	48	64	80	36	54	72	90	40	60	80	100
2	16	24	32	40	16	24	32	40	18	27	36	45	20	30	40	50
3	8	12	16	20	-	-	-	-	12	18	24	30	-	-	-	-
4	6	-	12	-	8	12	16	20	-	-	-	-	10	-	20	-
6 (or 5)	4	6	8	10	-	-	-	-	6	9	12	15	8	12	16	20
8	-	-	-	-	4	6	8	10	-	-	-	-	-	-	-	-

Slot-pole $N_{aa} \backslash n_L$	$Z=72, P=3, q=4$				$Z=72, P=4, q=3$				$Z=72, P=6, q=2$				$Z=96, P=4, q=4$			
	4	6	8	10	4	6	8	10	4	6	8	10	4	6	8	10
1	48	72	96	120	48	72	96	120	48	72	96	120	64	96	128	160
2	24	36	48	60	24	36	48	60	24	36	48	60	32	48	64	80
3	16	24	32	40	-	24	-	-	16	24	32	40	-	-	-	-
4	12	-	24	-	12	18	24	30	12	18	24	30	16	24	32	40
6	8	12	16	20	-	12	-	-	8	12	16	20	-	-	-	-
8	-	-	12	-	6	9	12	15	-	-	-	-	8	12	16	20

For both hairpin and lap winding				For hairpin winding only				For lap winding only								

Phase shift can also be configured more than one round in specific cases by further splitting sub phase belts. As shown in Fig. 13(b) and (e), the 8-layer hairpin winding design can be regarded as the combination of 4 sub 2-layer layouts. With transposition achieved in each sub layout, phase shift could be flexibly assigned. It should be noted that the minimum number of layers covered by one independent sub layer needs to follow Eqn. (3)-(4). Hence, Fig. 13(b) and (e) correspond to maximum number of phase shift for layout type II and III, respectively. If further divided phase belts are preferred, the coil pitch needs to be changed periodically. Taking the layout in Fig. 13(c) as an example, all the blue dashed lines denote connections with long pitch of 7 slots on welding side, while most U-shaped pins on the insertion side span a short pitch of 5 slots (omitted). All the jumpers for layer change also follow a short pitch without phase shift. Meanwhile, phasor change is assigned through the single layer connection shown in green. Fig. 13(f) shows a similar design concept with layout type III, in which the jumpers only correspond to layer change (shown in purple) and phasor change (shown in yellow). The overall phase shift effect is simply achieved by long and short pitch connections from welding and insertion side, respectively.

It should be noted that from a winding configuration point of view, all layouts in Fig. 13 are identical in terms of armature reaction. However, with more rounds of phase shift, AC losses can be effectively reduced in the slots where conductors from different phases are located alternately with proximity effect weakened. Despite the advantage in AC loss reduction, the reliability of interphase insulation in these slots needs to be carefully considered. The pin shapes, corresponding number of pins for 3-phase winding, as well as coil pitch for these layouts are further summarized in Table II. It can be seen that 9 and 7 pin shapes are needed for layout type II and III, respectively, excluding terminals.

D. Slot-pole combinations

Based on AC winding theory and Eqn. (3)-(7), typical slot-pole combinations suitable for hairpin winding configuration and EV traction motors are summarized in Table III, with of layer (conductor) number per slot n_L , parallel branch number N_{aa} listed as flexible options. The turn number in series per phase N_s is then calculated and highlighted in this table as the

key parameter which would influence the overall motor performance. The combinations which regular lap windings can be applied to are also marked for comparison. It is interesting to find that the configuration options of hairpin winding and random lap winding are not completely overlapping even with same slot-pole combination. Based on the “neighbouring layer” connection concept as discussed above, a parallel branch number of 3 or multiple of 3 which work for lap windings cannot be achieved in most cases of hairpin winding design.

Meanwhile, the multi-layer characteristic of hairpin winding brings additional design freedom compared to single or double layer lap windings. Hence, as shown in Table III, there are some combinations that can only work for hairpin windings or lap windings, respectively. Moreover, there are only a few options with turn number in series per phase suitable for EV traction motors with specific torque-speed range, power density level as well as kVA limitation on inverter side. Specifically, with the typical motor performance requirements of 150-250kW peak power, ≥ 15 krpm peak speed, as well as ≥ 600 V DC bus voltage for pure EV traction, the promising hairpin winding options are marked in red within Table III.

It should also be noted that for hairpin winding design, shifting towards higher number of q is challenging due to the difficulty in transposition. Although there are quite a few $q=3$ and $q=4$ cases as listed in Table III theoretically, the design flexibility is in fact significantly reduced due to much more pin shapes needed and higher risk of interference in end-winding modelling. In the following section, improved hairpin winding layout designs with higher number of q will be discussed in detail.

IV. NOVEL WINDING LAYOUTS WITH INCREASED SLOT NUMBER PER POLE PER PHASE

With design trends of traction machines moving to higher peak speeds and wider CPSR (constant power speed range), suppression of AC effects under high speed operation becomes more critical. Therefore, it is always beneficial to have lower conductor height and width for hairpin winding design on condition that the slot fill factor is not considerably impacted. Conductor height can be reduced by increasing the layer number, which can be flexibly configured. On the other hand,

conductor width reduction would lead to an increased slot number. With $q=2$ as discussed above, the pole number will then increase accordingly and offset the AC effect reduction due to the resulting higher operational frequency. High pole number will also challenge the switching capability of the inverter. Hence, a suitable solution would be a higher number of slots per pole per phase, such as the 54-slot, 6-pole combination adopted by Tesla Model 3 [2].

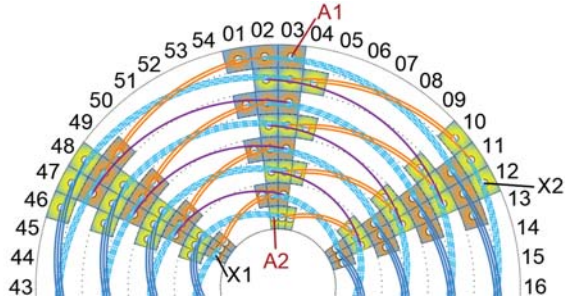


Fig. 14. Hairpin winding layouts with 54-slot, 6-pole, 8-layer, $N_{aa}=2$ [12].

For hairpin winding design, shifting towards higher number of q is challenging due to the difficulty in transposition. Although there are quite a few $q=3$ and $q=4$ cases theoretically as listed in Table III, design flexibility is in fact significantly reduced due to much more pin shapes needed and higher risk of interference in end-winding modelling. Within the three basic winding layouts discussed in the previous section, only type III is feasible for designs with $q=3$ or higher. Type I and II would lead to multiple intersections in layout connection which is not practical from a manufacturing point of view. An example of the existing solution of type III with $q=3$ is shown in Fig. 14 [12]. It is a 54-slot, 6-pole, 8-layer, short pitch case with $N_s=36$, $N_{aa}=2$, which falls into the feasible range as listed in Table III for high power density EV traction machines. This layout follows the design logic of covering all corresponding phasors between each pair of neighboring layers before moving to the next layer. Hence, compared with the case in Fig. 13(f), there are two jumpers of phasor change to achieve $q=3$. However, it can be clearly seen that the maximum parallel branch number per phase is limited to $N_{aa}=2$ with this method. In order to obtain layout solutions with higher N_{aa} , breakthrough solutions are needed.

In this section, two novel hairpin winding layouts are proposed to achieve higher number of both q and N_{aa} which allows for increased slots and layers for AC loss reduction. The core design philosophy is “multiplex”. As introduced in Sections II and III, there are majority of regular pins and minority of jumpers in a compete layout design. If a regular pin can achieve the function of a jumper at the same time, the total pin shapes needed can be effectively reduced. In other words, by fully utilizing the flexibility of jumpers, regular pins could be eliminated which significantly simplifies the configuration. This concept has been applied into the proposed layout case 1 and 2, which are focused on multiplexing of phasor change and layer change, respectively.

One specific embodiment of the proposed layout solution No. 1 is shown in Fig. 15, with $Z=56$, $p=3$, $N_{aa}=3$ and equivalent coil pitch of 8. It should be noted that the layer number is flexible, while selected as 10 only to make $N_s=30$ and falls into the feasible range listed in Table III. The connections on

welding side are the same with those in Fig. 14 and omitted. The slot-layer distribution corresponding to one phase is divided into 3 colours to denote different branches. This design combines the regular pins and jumpers of phasor change.

Take layer L_1 and L_2 of branch A1-X1 as example, the first welding connection spans 10 slots from S_{03-L_1} to S_{13-L_2} , while the following insertion connection spans 7 slots from S_{13-L_2} to S_{20-L_1} . Hence, one pair of welding and insertion connection covers only 17 slots, 1 slot less than a full pole pair spanning. Normally, this combination is not reasonable as the periodicity of wave winding cannot be maintained. Nevertheless, this asymmetric connection pair is exactly assigned for phasor change. The connection pair of S_{20-L_1} to S_{30-L_2} , and S_{30-L_2} to S_{37-L_1} corresponds to another round of phasor change. Further, the combination of S_{37-L_1} to S_{47-L_2} , and S_{47-L_2} to S_{03-L_1} achieves layer change and phasor “reset”. It can be seen that all the “regular” pins are with short pitch of 7 slots to continuously change the phasor. The other layers simply repeat this configuration and thus layer number could be flexibly selected.

The limitation of this method is that the number of q needs to be identical with pole pair p , as otherwise the number of phasor change will be either lower or higher than needed. Hence, the feasible slot-pole combination is restricted to $Z=24$, 54, 96..., with $p=2, 3, 4$..., respectively. Moreover, the maximum parallel branch number as listed in Table III can be achieved. Specifically, N_{aa} could be 6 for proposed case 1, while $N_{aa}=3$ is configured in Fig. 15 by connecting sub branches in series via the single layer pins marked in dark green.

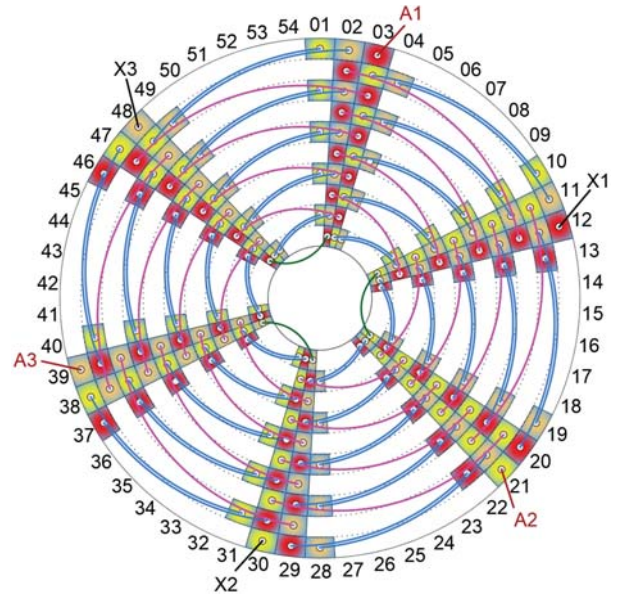


Fig. 15. Proposed layout solution No. 1 with 54-slot, 6-pole, 10-layer, $N_{aa}=3$.

Accordingly, the proposed layout solution No. 2 is focused on flexibility of layer change instead of phasor change. Fig. 16 gives an embodiment with the same number of slot, pole, layer and parallel branch as those in Fig. 15. The design concept is to continuously change layers and cover all of them as soon as possible with minimum number of pins. Thereafter, there will be more design freedom for the phasor change to be considered. Take the case in Fig. 16 for example, the connection from A1 follows S_{03-L_1} , S_{13-L_2} , S_{21-L_3} , S_{31-L_4} , S_{39-L_5} , S_{49-L_6} , S_{03-L_7} , S_{13-L_8} , S_{21-L_9} , $S_{31-L_{10}}$, from first layer gradually to bottom layer.

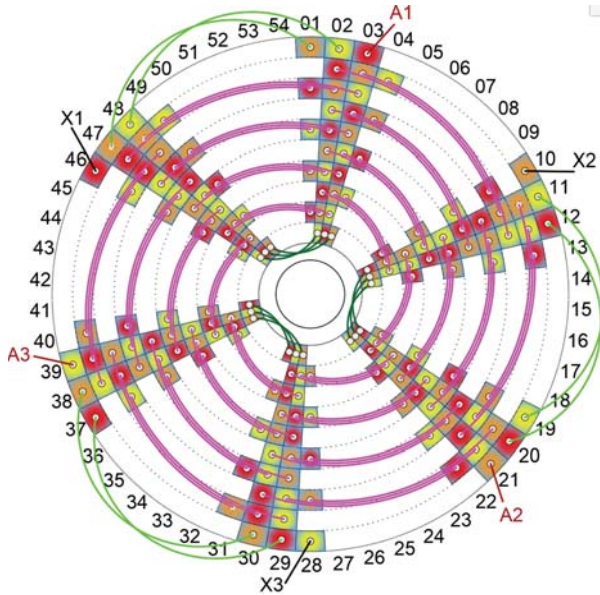


Fig. 16. Proposed layout solution No. 2 with 54-slot, 6-pole, 10-layer, $N_{aa}=3$.

Then, single layer connections from insertion side are assigned to allow for more revolutions between bottom and first layer, which can be allocated as jumpers for phasor change. Specifically for $N_{aa}=3$, the last layer pins are with full pitch, while the first layer ones are jumpers with short pitch and change phasors twice for each branch in this $q=3$ design. It should be noted that despite the intersections as shown in last and first layers of Fig. 16, interference of corresponding pins can be avoided through careful 3D shaping. All the other pins are jumpers of layer change with short pitch of 8 slots. By combining the welding connections which all span 10 slots uniformly, all the intermediate layers cover full pole pair pitch of 18 slots without equivalent phasor change.

By comparing the two novel winding layouts, it can be seen from distribution of each branch (shaded with same colour) that transposition is achieved in a different way, while both by covering all conductors needed to form complete phase belts. Meanwhile, all the jumpers of layer change can be switched to anti-clockwise direction as illustrated in Fig. 6 for design flexibility. Moreover, there are in total 10 and 6 different pin shapes needed excluding terminals and neutral points for the two layouts, which are even reduced compared with the cases of $q=2$ discussed in previous sections. Therefore, the two proposed solutions for higher number of q are practical and cost-effective from manufacturing point of view.

V. MULTI-PHYSICS DOMAIN MACHINE DESIGN AND PERFORMANCE COMPARISON

In this section, the typical 48-slot, 8-pole and the proposed 54-slot, 6-pole hairpin winding layouts discussed above will be applied to a specific interior PM (IPM) motor for further evaluation. Table IV gives basic parameters and performance requirements of the two machines prior to optimization. The upper limit of stator outer diameter (OD) is 210mm, which is reasonable for EV machines with 18000rpm peak speed due to the compromise needed between electromagnetic and rotor mechanical design. The pre-set performance indexes of power, speed, torque and CPSR are all typical for a compact EV.

Parameters	48-slot, 8-pole	54-slot, 6-pole
Winding layer number	8	10
Parallel branch number	2	3
Stator outer diameter, mm		≤ 210
Axial length, mm		100
Airgap length, mm		0.8
Peak power, kW		150
Peak speed, rpm		18000
Speed at knee point, rpm		5000
Peak torque, Nm		270
CPSR		≥ 3.5
Peak rms phase current, A		300
DC bus voltage, V		650
Magnet material		N38UH (100°C)
Winding material		Pure copper (150°C)

It should be noted that the turn number in series per phase N_s needs to be carefully designed among the inherently limited options for hairpin windings. With specific kVA rating on inverter side, N_s influences the shape of torque-speed curve especially CPSR to a large extent as it is related to both PM flux linkage and dq -axis inductance [39]. On the other hand, N_s needs to be selected from Table III, determined by slot, layer, and parallel branch number with consideration on conductor size and AC loss level. In this paper, $N_s=32$ and 30 are configured for 48-slot, 8-pole and 54-slot, 6-pole cases respectively.

Based on globally parametric modelling, a multi-physics design platform has been established with Jmag-Designer and ModeFRONTIER. Detailed optimization process is not the focus of this paper and will only be highlighted regarding the conductor size selection. The flux density and rotor von-Mises stress plots of the optimized cases are shown in Fig. 17 and 17, respectively.

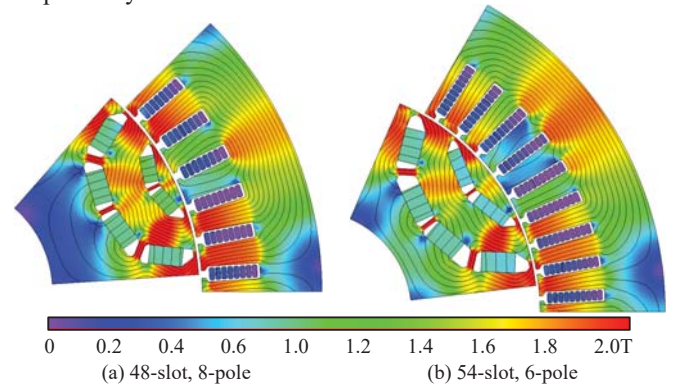


Fig. 17. Flux density contour plots under peak torque operation.

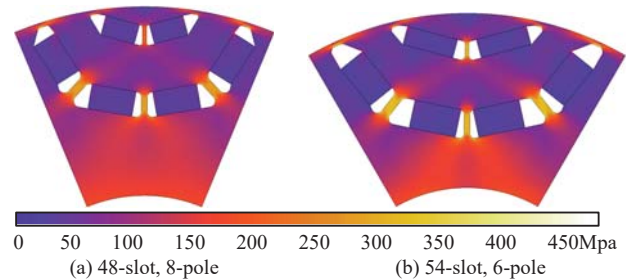


Fig. 18. Rotor Mises stress contour plots with peak speed of 18000rpm.

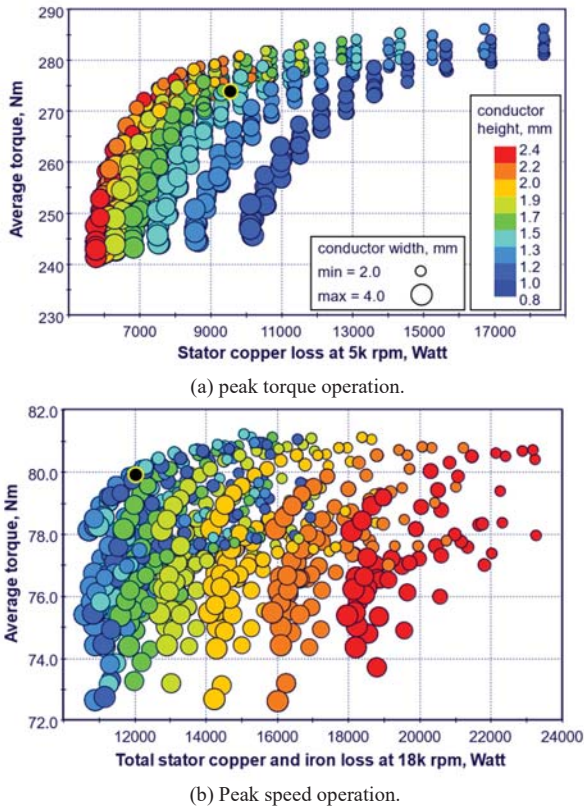


Fig. 19. Conductor size sifting of the 48-slot, 8-pole case.

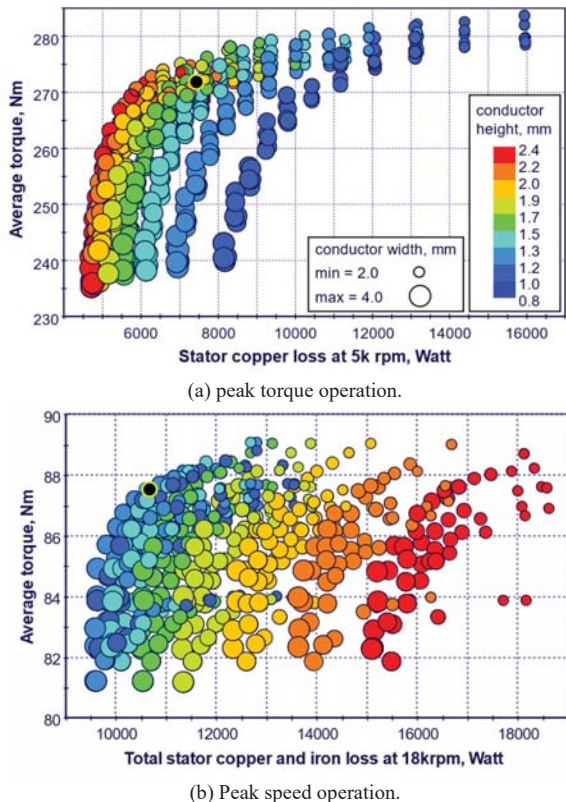


Fig. 20. Conductor size sifting of the 54-slot, 6-pole case.

With higher slot and layer number, it is straightforward to infer that the 54-slot, 6-pole design might lead to lower winding losses due to reduced conductor size compared with the 48-slot,

8-pole case. Nevertheless, more interesting conclusion can be found through quantitative sifting of conductor size. Fig. 19 and 19 illustrate the variation of output torque and power losses along with conductor size at knee point and peak speed for both machine designs, respectively. AC loss and end winding loss have been included in the calculation. In each specific figure, the feasible conductor sizes are located in the “pareto front” with high average torque but relatively low winding loss. Taking the peak torque operation of the 48-slot, 8-pole case shown in Fig. 19(a) as an example, for 270Nm peak torque, conductor with 3.2mm width and 2.2mm height seems to be the optimum option with 7kW winding loss. However, the same conductor size would lead to >17kW stator loss for the high power peak speed operation as shown in Fig. 19(b), which is not acceptable from a thermal management point of view. It can be further seen from Fig. 19(a) and (b) that the significant difference between low and high speed operation in terms of AC to DC copper loss ratio leads to almost opposite sifting results of conductor size. Hence, the conductor size of 3.4mm*1.4mm highlighted as black in the plot has been selected to balance the low and high speed performance.

Fig. 20 gives similar variation trends based on the 54-slot, 6-pole design. In Fig. 19(a) and Fig. 30(a) the same ampere-turns are applied for relatively fair comparison. Similar arrangements are also made for MTPV operation as shown in Fig. 19(b) and Fig. 20(b). As shown in Fig. 20(a) and (b), although pareto front regions of conductor size for low and high speed operation still cannot merge, their gap in between is reduced compared with the 48-slot, 8-pole case. Moreover, the selected conductor size of 2.8mm*1.4mm also corresponds to lower losses for both cases. It should be noted that only the peak torque and speed operation are investigated, as generally they will challenge the cooling system.

Fig. 21 further illustrates the comparison of efficiency maps based on the sifted 54-slot and 48-slot designs. For each design, winding loss with AC effect considered and iron loss with build factor of 1.5 have been calculated via FEA of ~5000 operating points based on the “accuracy mode” efficiency map function of Jmag-Designer. Another 20W/krpm mechanical loss has also been added for reasonable assumption of windage and stray effect. On the inverter side, 650V DC bus voltage and 300rmsA peak phase current have been configured. The peak torque of the 48-slot design is higher than that of the 54-slot case mainly due to its slightly higher turns in series per phase N_s (higher current loading under the same peak current). Meanwhile, with lower ratio of PM flux linkage to d -axis inductance, the output power capability of the 48-slot case in high speed region is not as good as that of the 54-slot case [41]. More specifically, it can be see that the 54-slot case shows relatively wider range of high efficiency area. By summarizing the power loss data, it is found that the winding loss as dominant loss component, is higher in major operating points for the 48-slot design. This is led by ~15% less copper area compared with the 54-slot design. By increasing the conductor size, the efficiency of the 48-slot design will be improved in low-speed region, while AC copper loss will be significantly increased along with rotation speed, which then deteriorates the efficiency in high-speed, high-power region. More importantly, the resultant high copper loss density especially near the slot opening area will challenge the cooling capability.

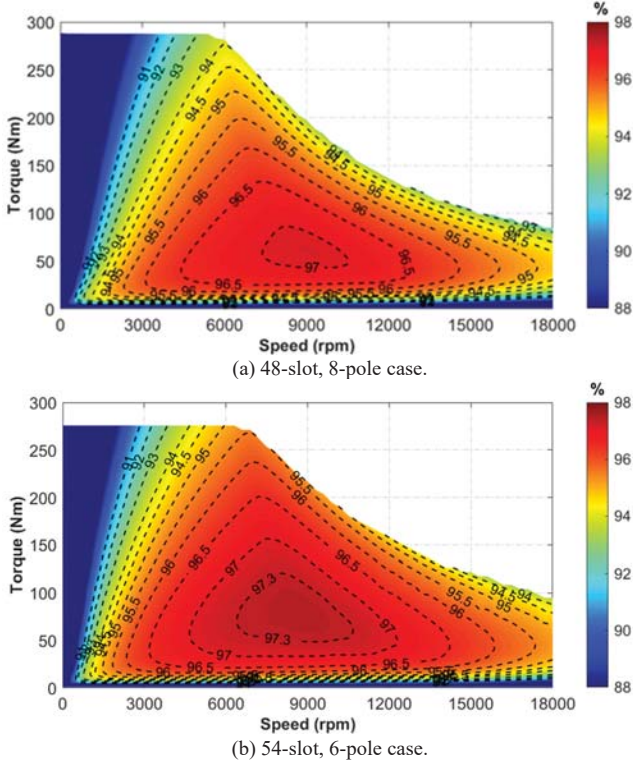


Fig. 21. Comparison of the efficiency maps between the selected 48-slot, 8-pole and 54-slot, 6-pole cases.

It should be noted that in this paper, the optimization process for the hairpin winding motor designs is power density instead of efficiency driven. Hence, the focus has been put on reducing and balancing the power losses in the most challenging scenarios such as peak torque and peak speed. There are other representative operation points to be covered for an industrial level traction machine development, and driving cycle efficiency needs to be carefully considered to improve the overall mile per gallon (MPG) of the vehicle in city and/or highway driving. Hence, it's not intended to draw the conclusion in this paper that 54-slot, 6-pole combination is always a better solution than the 48-slot, 8-pole counterpart. Meanwhile, the proposed hairpin winding layout with higher number of q has been verified as a promising candidate for power density and efficiency improvement of high speed traction motors.

Thermal analysis based on the selected 48-slot, 8-pole and 54-slot, 6-pole designs is conducted by means of computational fluid dynamics (CFD). External water jacket cooling and internal oil spray delivered by high pressure nozzles are combined to work on the heat generated from stator core and end windings, respectively. Meanwhile, the detailed power loss components of the two counterparts have been extracted as thermal inputs, especially the copper loss from each layer of hairpin conductors. With the same cooling capability, the contour plots of temperature rise (captured from middle section of the CFD model) with respect to coolant inlet for peak operations are shown in Fig. 22 for the 48-slot case and Fig. 23 for the 54-slot case, respectively. It can be seen that the 54-slot case corresponds to around 30°C reduced peak temperature rise due to much lower losses. The performance comparison of the two machine designs is further listed in Table V.

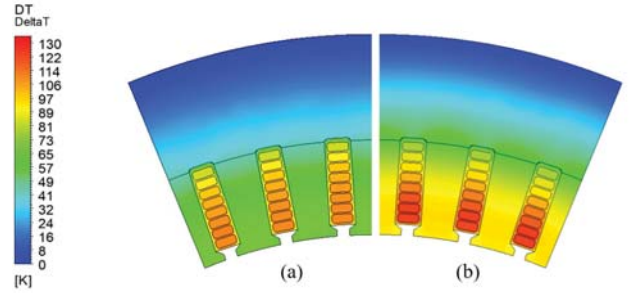


Fig. 22. Temperature rise based on CFD analysis of the 48-slot, 8-pole case for: (a) peak torque operation at 5000rpm. (b) peak speed operation.

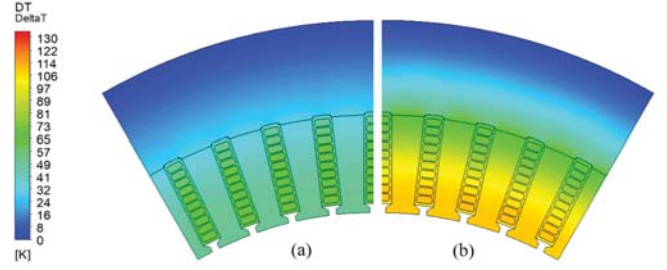


Fig. 23. Temperature rise based on CFD analysis of the 54-slot, 6-pole case for: (a) peak torque operation at 5000rpm. (b) peak speed operation.

TABLE V
PERFORMANCE COMPARISON FOR PEAK OPERATION

Slot-pole combination	48-slot, 8-pole		54-slot, 6-pole	
Parameters	5krpm	18krpm	5krpm	18krpm
RMS current * N_s , kA	9.0	6.6	9.0	6.6
Current density, A/mm ²	29.5	21.7	25.5	18.7
Average torque, Nm	273.5	79.7	271.8	87.6
Torque ripple, 100%	8.0%	31.4%	2.9%	10.3%
Copper loss, kW	9.2	7.8	7.4	5.6
Total to DC loss ratio	1.05	1.66	1.05	1.38
Stator iron loss, kW	0.8	4.4	0.6	5.5
Stator outer diameter, mm	210.0		210.0	
Rotor outer diameter, mm	139.0		134.4	
Conductor size, mm*mm	3.4*1.4		2.8*1.4	
Magnet usage, kg	1.42		1.48	

VI. MANUFACTURING OF THE PROTOTYPE

Based on the proposed hairpin winding layout concept as shown in Fig. 16 and the conductor size sifting discussed above, detailed 3D winding assembly has been modelled with careful consideration on reduction of end turn length, reliability of manufacturing as well as cooling arrangement. The finalized drawing was then released for prototyping. Prior to be bent into specific shapes, rectangular conductors with selected size needs to go through straightening, stripping, and cutting process. Fig. 24 shows several individual pins through CNC manipulation. Then, the pins with the same shapes were put into specific carrier to be aligned and further inserted into the stator with slots covered by insulation papers. On the other side of the stator, the pins further went through widening, twisting, welding, trickling, and finally followed by whole stator impregnation. The insertion side and welding side of the full stator prototype is shown in Fig. 25 as validation of the proposed hairpin winding layout.

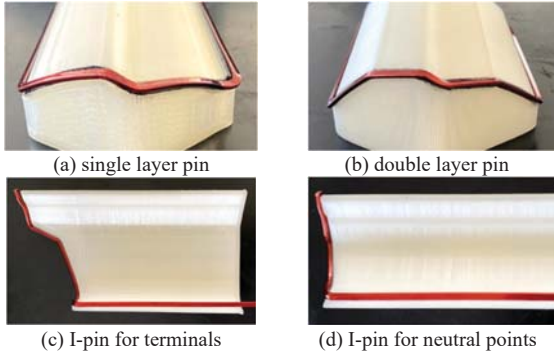


Fig. 24. Different types of pins for the proposed hairpin winding prototype.

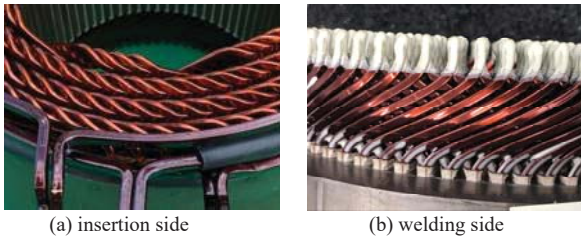


Fig. 25 Insertion and welding side views of the hairpin winding stator prototype.

Based on the hairpin winding stator prototype, the line (phase) resistance values have been measured. Moreover, all the branch resistance values (branch terminal to neutral point) have also been tested to validate, in order to eliminate the concerns of unbalanced resistance distribution due to potential welding issue. Corresponding per-unit data (tested value/design value) are summarized in Table VI. It can be seen that all the measured line and branch resistance agree well with the designed values. Hence, the accuracy and consistency of the manufacturing process have been further verified.

Table VI Tested line and branch resistance (per-unit value based on design)

Line resistance		Branch resistance					
Items	value	Items	value	Items	value	Items	value
AB	1.003	A1	1.000	A2	1.006	A3	1.002
BC	1.002	B1	1.000	B2	1.001	B3	1.004
CA	1.003	C1	1.000	C2	1.005	C3	1.003

VII. CONCLUSION

In this paper, the design philosophy of hairpin winding layouts has been comprehensively presented. The flexibility of end-winding connection has been thoroughly investigated in terms of basic pin connections and special jumpers with focus on transposition. The diversity in allocating parallel branches, terminal positions, phase shift as well as winding pitches have also been evaluated. Conclusion has been drawn that a balance between winding performance and manufacturing cost needs to be reached among various options jumper arrangement. Promising winding layout candidates have been sifted out based on specific case study of 48-slot, 8-pole windings. Based on the summarized slot-pole combinations, the flexibility and limitation in hairpin winding design is further evaluated and also compared with conventional lap windings. It has also been pointed out that windings with higher number of q ($q > 2$) is preferred for high power density traction motors, while corresponding layout solutions are limited.

Two novel hairpin winding designs with increased slot number per pole per phase are proposed for industrial level EV

traction motors, addressing directly limitations with existing layouts. The core design philosophy is “multiplex” of jumpers which could significantly reduce the number of pin shapes needed. A 160kW, 18000rpm interior PM traction motor with 54-slot, 6-pole is designed using the proposed layout and optimized within a multi-physics platform which puts special attention on conductor size selection. The advantages of the designed motor in both electromagnetic and thermal performance have been clearly revealed by comparison to a more traditional 48-slot, 8-pole counterpart. Finally, a corresponding stator prototype with the proposed hairpin winding solution has been built and its manufacturability has been validated.

VIII. ACKNOWLEDGEMENT

The authors would like to thank JSOL for providing Jmag-Designer as powerful FEA packages for machine optimization.

REFERENCES

- [1] C. Grayling, *et al.*, “The Road to Zero: Next steps towards cleaner road transport and delivering our Industrial Strategy,” Department for Transport, London, UK, July 2018. [Online] Available: https://assets.publishing.service.gov.uk/government/uploads/system/uploads/attachment_data/file/739460/road-to-zero.pdf.
- [2] I. Husain *et al.*, “Electric Drive Technology Trends, Challenges, and Opportunities for Future Electric Vehicles,” in *Proceedings of the IEEE*, vol. 109, no. 6, pp. 1039-1059, June 2021.
- [3] C. Shaw, *et al.*, “Electric vehicles: driving the transition”, Fourteenth Report of Session 2017–19, Business, Energy and Industrial Strategy Committee, House of Commons, UK, Oct 2018.
- [4] 2020 Annual Merit Review Report, Vehicle Technologies Office (VTO), Department of Energy (DOE), USA, June 2020. [Online] Available: <https://www.energy.gov/eere/vehicles/downloads/2020-annual-merit-review-report>.
- [5] N. Jackson, B. Mecrow, *et al.*, “Electric Machines Roadmap 2020”, Advanced Propulsion Centre (APC), UK, Feb 2021, [Online] Available: <https://www.apcuk.co.uk/technology-roadmaps/>.
- [6] T. Burress, *et al.*, “Electrical Performance, Reliability Analysis, and Characterization”, DOE Vehicle Technologies Office Annual Merit Review, USA, June 2017.
- [7] A. M. El-Refai, “Motors/generators for traction/propulsion applications: A review,” in *IEEE Vehicular Technology Magazine*, vol. 8, no. 1, pp. 90-99, March 2013.
- [8] D. Staton, J. Goss, “Open Source Electric Motor Models for Commercial EV & Hybrid Traction Motors”, presented at Exhibition of Coil Winding, Insulation & Electrical Manufacturing Exhibitions (CWIEME), Berlin, Germany, June 2017.
- [9] A. Bardalai *et al.*, “Reduction of Winding AC Losses by Accurate Conductor Placement in High Frequency Electrical Machines,” in *IEEE Transactions on Industry Applications*, vol. 56, no. 1, pp. 183-193, Jan.-Feb. 2020.
- [10] M. Popescu, J. Goss, D. A. Staton, D. Hawkins, Y. C. Chong and A. Boglietti, “Electrical Vehicles—Practical Solutions for Power Traction Motor Systems,” in *IEEE Transactions on Industry Applications*, vol. 54, no. 3, pp. 2751-2762, May-June 2018, doi: 10.1109/TIA.2018.2792459.
- [11] W. Cai, D. Fulton and C. L. Congdon, “Multi-set rectangular copper hairpin windings for electric machines,” U. S. Patent 7034428 B2, Apr. 22, 2006.
- [12] W. Cai, “Terminals and Connections Between Multi-Set Segmented Hairpin Windings”, U. S. Patent 7622843 B2, Nov. 24, 2009.
- [13] F. Momen, K. Rahman and Y. Son, “Electrical Propulsion System Design of Chevrolet Bolt Battery Electric Vehicle,” in *IEEE Transactions on Industry Applications*, vol. 55, no. 1, pp. 376-384, Jan.-Feb. 2019, doi: 10.1109/TIA.2018.2868280.
- [14] S. Sano, T. Yashiro, K. Takizawa, T. Mizutani, “Development of New Motor for Compact-Class Hybrid Vehicles”, *World Electric Vehicle Journal*. 2016; 8(2): 443-449.
- [15] T. Dimier, M. Cossale and T. Wellerdieck, “Comparison of Stator Winding Technologies for High-Speed Motors in Electric Propulsion

- Systems,” *2020 International Conference on Electrical Machines (ICEM)*, 2020, pp. 2406-2412.
- [16] Y. Zhao, D. Li, T. Pei and R. Qu, “Overview of the rectangular wire windings AC electrical machine,” in *CES Transactions on Electrical Machines and Systems*, vol. 3, no. 2, pp. 160-169, June 2019.
- [17] T. Ishigami, Y. Tanaka and H. Homma, “Motor Stator With Thick Rectangular Wire Lap Winding for HEVs,” in *IEEE Transactions on Industry Applications*, vol. 51, no. 4, pp. 2917-2923, July-Aug. 2015.
- [18] Y. Wang, J. Pries, K. Zhou, H. Hofmann and D. Rizzo, “Computationally Efficient AC Resistance Model for Stator Winding With Rectangular Conductors,” in *IEEE Transactions on Magnetics*, vol. 56, no. 4, pp. 1-9, April 2020, Art no. 8100509.
- [19] D. P. Morisco, S. Kurz, H. Rapp and A. Möckel, “A Hybrid Modeling Approach for Current Diffusion in Rectangular Conductors,” in *IEEE Transactions on Magnetics*, vol. 55, no. 9, pp. 1-11, Sept. 2019, Art no. 8002111.
- [20] M. Aoyama and J. Deng, “Visualization and quantitative evaluation of eddy current loss in bar-wound type permanent magnet synchronous motor for mild-hybrid vehicles,” in *CES Transactions on Electrical Machines and Systems*, vol. 3, no. 3, pp. 269-278, Sept. 2019.
- [21] G. Venturini, G. Volpe, M. Villani and M. Popescu, “Investigation of Cooling Solutions for Hairpin Winding in Traction Application,” *2020 International Conference on Electrical Machines (ICEM)*, 2020, pp. 1573-1578.
- [22] F. Zhang *et al.*, “A Thermal Modelling Approach and Experimental Validation for an Oil Spray-Cooled Hairpin Winding Machine,” in *IEEE Transactions on Transportation Electrification*, doi: 10.1109/TTE.2021.3067601.
- [23] C. Liu *et al.*, “Experimental Investigation on Oil Spray Cooling With Hairpin Windings,” in *IEEE Transactions on Industrial Electronics*, vol. 67, no. 9, pp. 7343-7353, Sept. 2020.
- [24] P. Mancinelli, S. Stagnitta and A. Cavallini, “Qualification of Hairpin Motors Insulation for Automotive Applications,” in *IEEE Transactions on Industry Applications*, vol. 53, no. 3, pp. 3110-3118, May-June 2017.
- [25] C. He, C. P. Beura and S. Tenbohlen, “Investigation of Partial Discharge Activity in the Slot of a Hairpin-wound Stator,” *2020 International Symposium on Electrical Insulating Materials (ISEIM)*, 2020, pp. 565-568.
- [26] F. Wirth and J. Fleischer, “Influence of Wire Tolerances on Hairpin Shaping Processes,” *2019 9th International Electric Drives Production Conference (EDPC)*, 2019, pp. 1-8, doi: 10.1109/EDPC48408.2019.9011999.
- [27] T. Glaessel, J. Seefried and J. Franke, “Challenges in the manufacturing of hairpin windings and application opportunities of infrared lasers for the contacting process,” *2017 7th International Electric Drives Production Conference (EDPC)*, 2017, pp. 1-7.
- [28] D. Mayer, L. Hausmann, N. Maul, L. Reinschmidt, J. Hofmann and J. Fleischer, “Systematic Investigation of the Grooving Process and its Influence on Slot Insulation of Stators with Hairpin Technology,” *2019 9th International Electric Drives Production Conference (EDPC)*, 2019, pp. 1-7.
- [29] J. Vater, P. Schlaak and A. Knoll, “A Modular Edge-/Cloud-Solution for Automated Error Detection of Industrial Hairpin Weldings using Convolutional Neural Networks,” *2020 IEEE 44th Annual Computers, Software, and Applications Conference (COMPSAC)*, 2020, pp. 505-510.
- [30] G. Berardi and N. Bianchi, “Design Guideline of an AC Hairpin Winding,” *2018 XIII International Conference on Electrical Machines (ICEM)*, 2018, pp. 2444-2450.
- [31] N. Bianchi and G. Berardi, “Analytical Approach to Design Hairpin Windings in High Performance Electric Vehicle Motors,” *2018 IEEE Energy Conversion Congress and Exposition (ECCE)*, 2018, pp. 4398-4405.
- [32] K. M. Rahman, E. L. Kaiser, S. Jurkovic, P. J. Savagian, “Stator assembly with winding sets having hairpins from multiple hairpin layers”, U. S. Patent 9520753B2, Dec. 13, 2016.
- [33] D. Han, M. K. Jeong, Y. J. Seo, H. Cho, “Stator winding pattern for hairpin drive motor”, U. S. Patent 9876406B2, Jan. 23, 2018.
- [34] M. Awazu, K. Okada, I. Nitta, H. Shimozu, “Rotating Electrical Machine And Method Of Manufacturing Same”, U. S. Patent 10305339B2, May. 28, 2019.
- [35] T. Berger, C. Schwarzkopf, “Method for producing a bar winding for the stator of an electric machine”, U. S. Patent 8584346B2, Nov. 19, 2013.
- [36] M. S. Islam, I. Husain, A. Ahmed and A. Sathyan, “Asymmetric Bar Winding for High-Speed Traction Electric Machines,” in *IEEE Transactions on Transportation Electrification*, vol. 6, no. 1, pp. 3-15, March 2020.
- [37] Y. Zhao, D. Li, T. Pei and R. Qu, “Variable Turn Rectangular Wire Winding Permanent Magnet Machine,” *2020 International Conference on Electrical Machines (ICEM)*, 2020, pp. 366-372.
- [38] F. Endert, T. Heidrich, U. Schwalbe, T. Szalai and S. D. Ivanov, “Effects of current displacement in a PMSM traction drive with single turn coils,” *2013 International Electric Machines & Drives Conference*, 2013, pp. 160-165.
- [39] Aumann AG. 2021. *Hairpin stators*. [online] Available at: <https://www.aumann.com/en/services/industry-solutions/e-mobility-automotive/electric-drive/hairpin-stators/>.
- [40] Additive Drives. 2021. *E-Traction Motor - Additive Drives*. [online] Available at: <https://www.additive-drives.de/en/project/e-traction-motor/>.
- [41] N. Bianchi and T.M. Jahns, “Design analysis and control of interior PM synchronous machines”, presented at the *IEEE Industry Applications Society Annual Meeting*, Seattle, USA, October 3rd, 2004. pp 2.14–2.18.